Food Structure 37 (2023) 100330

Contents lists available at ScienceDirect

Food Structure

journal homepage: www.elsevier.com/locate/foostr

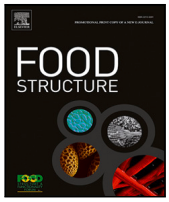

Heterogeneous swelling of couscous particles exposed to a high relative humidity air, as revealed by TD-NMR and X-ray tomography

Ilija Vego [a,*], Richard T. Benders [b], Alessandro Tengattini [a,c], Frank J. Vergeldt [d], Joshua A. Dijksman [b,e], John P.M. van Duynhoven [d,f]

[a] Univ. Grenoble Alpes, Grenoble INP, CNRS, 3SR, F-38000 Grenoble, France
[b] Physical Chemistry and Soft Matter, Wageningen University & Research, Stippeneng 4, 6708 WE, Wageningen, The Netherlands
[c] Institut Laue-Langevin (ILL), 71 Avenue des Martyrs, 38000 Grenoble, France
[d] Laboratory of Biophysics, Wageningen University & Research, Stippeneng 4, 6708 WE Wageningen, The Netherlands
[e] Van der Waals-Zeeman Institute, Institute of Physics, University of Amsterdam, Science Park 904, 1098 XH Amsterdam, The Netherlands
[f] Unilever Global Foods Innovation Centre, Plantage 14, 6708 WJ Wageningen, The Netherlands

ARTICLE INFO

Keywords:
Couscous particles
Hygroscopic
Free swelling
TD-NMR
X-ray tomography

ABSTRACT

The mechanical behaviour of hygroscopic granular materials is highly influenced by water. The strong dependence of individual particle properties on moisture content affects the response of their packings, which can agglomerate and eventually lead to loss of product functionality. Despite the frequent occurrence of this problem in industry, only few studies tried to explore the underlying phenomena and investigate the fundamental connection between particle and packing behaviour. This work presents an experimental study that aims to link the water uptake to the microstructural changes in assemblies of couscous, a material selected to be representative of hygroscopic granular materials. In the experiments, the samples are exposed to high relative humidity (RH), and the moisture content increase is quantified with TD-NMR, along with the shift in molecular mobility. An analogous test is performed, during which x-ray tomographies are acquired continuously. We analyse the volumetric response of the sample and of thousands of particles. Despite the oversupply of water molecules available to saturate the system, the formation of a swelling heterogeneity is observed, which we attribute to the pressure gradient affecting locally the adsorption kinetics. Combining the results obtained from the two techniques, water uptake and particle swelling are found to be linearly correlated.

1. Introduction

The presence of water can significantly affect the behaviour of granular food products. Sugar, seeds, flour are some examples. These are all composed of individual "particles" or "grains" that interact with each other. Hydro-sensitive granular materials can be also found in pharmaceutical industry, where, despite the different application and chemical composition, analogous problems are encountered on a daily basis while processing or storing products.

One of the most common problems encountered during the handling and industrial processing of hygroscopic granular materials, is the accidental moisture content increase due to the mismatch in water activity of those materials with the environment. Water absorption can alter the material properties at the molecular scale, with repercussions at the particle- and, ultimately, the product-scale. The interaction of water molecules with polymer chains inside the hygroscopic materials (e.g., amylose and amylopectin starch chains (Stading, Rindlav-Westling, & Gatenholm, 2001) and protein matrix) affects their relaxation properties and alters various polymer properties like glass transition temperature T_g (Aguilera, del Valle, & Karel, 1995; Zafar, Vivacqua, Calvert, Ghadiri, & Cleaver, 2017). In granular media, this often translates into particle-scale phenomena such as swelling, release of mucilage, loss of mechanical properties, and creation of fissures. All these have direct effects on the bulk behaviour of the material. The particles can agglomerate or *cake*, a phenomenon that leads to lower product functionality and flowability (Aguilera et al., 1995; Carpin et al., 2016; Zafar et al., 2017).

Inefficiencies in the supply chain can cause significant loss of resources (Chauhan, Dhir, Akram, & Salo, 2021; Rathore & Winkle,

* Corresponding author.
E-mail addresses: ilija.vego@univ-grenoble-alpes.fr (I. Vego), richard.benders@wur.nl (R.T. Benders), alessandro.tengattini@3sr-grenoble.fr (A. Tengattini), frank.vergeldt@wur.nl (F.J. Vergeldt), joshua.dijksman@wur.nl (J.A. Dijksman), john-van.duynhoven@unilever.com (J.P.M. van Duynhoven).

https://doi.org/10.1016/j.foostr.2023.100330
Received 3 February 2023; Received in revised form 23 May 2023; Accepted 3 June 2023
Available online 9 June 2023

2009), which obviously raises economical and, most importantly, sustainability issues. However, despite the relevance and daily occurrence of the problem, very little is known about the individual particle to product relations, *i.e.*, multi-scale relations, which govern the material behaviour (Carpin et al., 2016; Fitzpatrick & Ahrné, 2005; Zafar et al., 2017).

Nuclear magnetic resonance (NMR) is a versatile, non-invasive method that can be used to analyse food stuff in real time at various length scales, ranging from their molecular structure up to the meso-scale (Hatzakis, 2019; van Duynhoven, Voda, Witek, & Van As, 2010). This technique can be used to understand the fundamental interactions between water and hygroscopic materials. NMR has been extensively used to study drying processes (Penvern et al., 2020), as well as the absorption of free water by couscous (De Richter et al., 2022). However, the use of time-domain NMR (TD-NMR) in water vapour-sorption from air at high humidity levels, has received little attention, despite its potential use in understanding the molecular processes that underlie agglomeration and caking in greater detail (Chung et al., 2000).

Several studies focused on the behaviour of individual particles. For example, within the domain of food industry, the effects of moisture content increase on the volume or mechanical properties of particles were investigated for lentil seeds (Amin, Hossain, & Roy, 2004), rice grains (Cao, Nishiyama, & Koide, 2004; Kamst, Bonazzi, Vasseur, & Bimbenet, 2002; Morita & Singh, 1979; Sadeghi, Araghi, & Hemmat, 2010; Sharma & Kunze, 1982), wheat kernels (Figueroa et al., 2011; Glenn, Younce, & Pitts, 1991; Tabatabaeefar, 2003), micro-crystalline cellulose (Shi, Feng, & Sun, 2011), and couscous (Abecassis, Cuq, Boggini, & Namoune, 2012; De Richter et al., 2022).

The bulk response of hygroscopic materials has also been investigated. For example, the flowability properties for lactose powder were found to be lower in highly dry or highly humid conditions (Lumay et al., 2016). Similar responses were observed for micro-crystalline cellulose, pectin, maltodextrin and starch powders (Crouter & Briens, 2014; Juarez-Enriquez et al., 2017). It was shown that a long exposure to humidity can increase the overall cohesion of different materials and that the agglomeration process is not homogeneous (Brockbank, Armstrong, & Clayton, 2021).

Few studies have explored the multi-scale relation between hygroscopicity and bulk behaviour. For example, Wahl et al. (2008) investigated with experiments and numerical simulations the caking "strength" of a fertiliser (urea prills). The inter-particle contact tensile strength was measured with respect to the "storage time", along with the increase of the contact area detected optically. The results were then used to build a contact-dynamics model, which was implemented to numerically simulate the bulk response. Haider et al. (2014) carried out experiments to investigate the inter-particle contact genesis in an amorphous reference hydro-sensitive reference material (maltodextrin dextrose) and the role that temperature plays over the contact mechanical strength and morphology. More recently, Vego, Tengattini, Andò, Lenoir, and Viggiani (2022) performed an oedometric test, *i.e.*, radial strain constrained and constant vertical stress, while exposing an assembly of couscous particles to a flow of high relative humidity air to activate the phenomena related to water absorption from the external environment. During the whole experiment, 4D images with X-ray tomography were acquired to explore the effects of humidity and characterise, through image analysis, the microstructural changes such as particle volume and inter-particle contacts, which were found to be correlated and strongly influenced by the applied boundary conditions.

The study of couscous particles can be of great interest, because of its increasing worldwide consumption and production, and also because many other products are made from the same wheat, *e.g.*, pasta (Hammami & Sissons, 2020). Moreover, when in contact with water, couscous presents several of the phenomena described above: its particles absorb water, swell, lose mechanical rigidity and eventually agglomerate (Abecassis et al., 2012; Bellocq, Ruiz, & Cuq, 2018; De Richter et al., 2022; Vego et al., 2022). Finally, according to *Codex Alimentarius*, couscous particles should have a diameter between 630 μm and 2 mm, which makes them well suited for particle scale measurement in images obtained from the X-ray tomography (Vego et al., 2022). Fine couscous (Ferrero, Groupe Panzani) is selected as a material of interest to perform the study presented in this paper, with the same rationale as in Vego et al. (2022). In this study, the average equivalent particle diameter was found to be 0.9 mm. Moreover, the typical fine couscous size distribution is more representative of the wide range of hygroscopic granular materials (Hammami, Barbar, Laurent, & Cuq, 2022), and it provides a larger statistical sample for particle scale measurements. We aim to explore its behaviour when particles are exposed to high relative humidity (RH) environments. By adopting TD-NMR we investigate the water uptake dynamics while also getting insights into whether water gets absorbed or condenses. The complementary use of X-ray tomography allows us to observe swelling kinetics of thousands of particles.

2. Material and methods

2.1. Gravimetric assessment: experimental procedure

The sorption isotherm of fine couscous is determined at room temperature (20.7 ± 0.5 °C), exposing the particles to air of different relative humidities. The sample mass is continuously recorded by an analytical balance placed inside a plastic, closed container, connected to an conditioned airline, which is equipped with a temperature and relative humidity (RH) sensor (Thorlabs, Inc TSP01 revB). The relative humidity of the air within the setup is servo-controlled by measuring the RH at the sample position and adjusting the humidity of the injected air though an ultrasonic humidifier (Beurer LB12). Specifically, the feedback loop turns on the humidifier when the RH-sensor measures values below the target, thus ensuring control of the RH within the sample chamber. The air pressure is maintained at equilibrium by small holes inside the plastic box, allowing excess air to leak into the surrounding environment.

Initially, the particles are exposed to low humidity air ($11.0 \pm 0.2\%$) for a period of 3 days. Lower RH levels could not be reached due to technical limitations. Afterwards, a series of 12 RH-increments every 24 h is performed, until reaching a $98.1 \pm 0.5\%$ RH, close to the saturation point of air. Smaller increments are applied when increasing low or high RH levels. The increase in relative humidity of the air, leads to the absorption of water by the couscous particles which is quantified by their change in mass.

Afterwards, the dry matter content m_{dry} of the couscous particles is determined by placing the material in a convection oven for 24 h at 105 °C. The weight loss is then assessed with respect to the mass at the beginning of the experiment (Rostom, Courtier-Murias, Rodts, & Care, 2020). The moisture content $m.c.$ is determined over the course of the experiment, following Eq. (1):

$$m.c. = \frac{m_{24h} - m_{dry}}{m_{dry}} \times 100\,[\%] \tag{1}$$

where m_{24h} is the mass after the 24 h exposure to a specific RH level.

2.2. TD-NMR relaxometry

2.2.1. Experimental procedure

At the start of the experiments, couscous particles are dried with a flow of 0% RH air at 21 °C for 3 days in a sealed vessel. Dry air is used to lower the couscous particles' moisture content, in order to prevent structural changes associated with thermal heating of the couscous in an oven.

Next, the particles are transferred into a custom cylindrical cell made of PTFE with an inner diameter of 7 mm. At the bottom of the probe cell a glass porous stone is placed allowing humid air to pass,

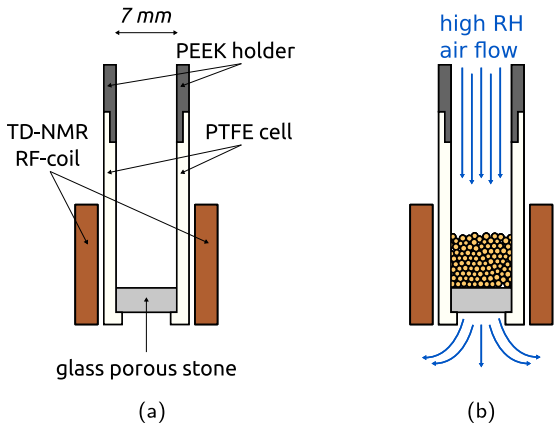

Fig. 1. Schematic view of the measurement cell used for the TD-NMR experiment (a). Sketch of experimental configuration (b). The couscous particles are placed in the cell, and attention is payed not to exceed the homogeneous region of the RF coil. A flow of high RH air is circulated through the sample.

while preventing the particles from falling out of the cell. During the experiments, the bed of particles is subjected to a 0.2 L/min flow of 97% RH air, supplied with the same RH unit described in Section 2.1. These experimental conditions are selected posterior a preliminary study presented in the (Appendix A). A schematic overview of the setup is shown in Fig. 1.

2.2.2. FID-CPMG decay acquistion

The ^{1}H NMR transversal relaxation decays are acquired using a combined Free Induction Decay (FID) and Carr–Purcell–Meiboom–Gill (CPMG) sequence (Carr & Purcell, 1954; Hahn, 1953; Meiboom & Gill, 1958). The first is often used to investigate crystalline or glassy materials, *e.g.*, sugar, characterised by a relatively short T_2 relaxation time, while the CPMG sequence is more suitable for the analysis of liquid-like components, associated with longer T_2 relaxation times (van Duynhoven et al., 2010).

In this study, the FID-CPMG decays are acquired using a low-field 20 MHz ^{1}H (0.47 T) Bruker Minispec MQ20 ND spectrometer equipped with a probehead with a deadtime of ≈11 μs. At this field strength measurements are sufficiently sensitive and the short deadtime allows for assessment of all relevant T_2 NMR relaxation times.

The measurement cell is lowered into the probe head and properly aligned, so that the sample resides within the homogeneous region of the radio-frequency (RF) coil. At the start of the experiment the empty cell is measured to obtain the background signal, *i.e.* signal not associated with the matrix inside the couscous particles (see Fig. 1(a)). Next, the dried particles are weighted and transferred into the cell.

The FID is sampled over 100 μs at a frequency of 2.5 MHz. The echo time (TE) of the CPMG sequence is 0.2 ms with a total of 50 echoes. The signal to noise ratio is increased by averaging over 8 scans, with a recycle delay of 8 s.

The sequence is performed 50 times over a period of 18 h, starting the first before the high air RH flow is switched on. The timing between the initial sequences is higher compared to those at end of the experiment, to accommodate for the faster change in water content in the early stages of the experiment. The experiment is performed in duplicate. Part of the last data points of the backup test (named here test "B") have been lost due to a data storage error.

2.2.3. FID-CPMG decay analysis

We analyse the FID-CPMG decays in terms of three main components: one corresponding to the solid fraction, which has a very low proton mobility and thus a short relaxation time T_2, one with the absorbed water fraction and one to the lipid plus eventual water droplets, with increasingly long T_2.

To analyse this signal, we subtract the background, and then, using the `scipy.optimize.curve_fit` function (Virtanen et al., 2020), we fit the FID-CPMG decay of magnetisation $M(t)$ with the empirical form:

$$M(t) = S\, e^{-0.5\left(\frac{-t}{T_{2,S}}\right)^2} + L\, e^{-\frac{t}{T_{2,L}}} + F \tag{2}$$

where S describes the overall amplitude of the solid-phase signal, characterised by the relaxation time $T_{2,S}$. The second term corresponds to the semi-solid and/or liquid-like fraction within the sample, with L describing its signal amplitude and $T_{2,L}$ its relaxation time. The last term F describes the components with long relaxation times, like oil and unbound water. This last term is expected to be constant throughout the experiment. The amount of oil cannot change along the experiment and no formation of water droplets or capillary bridges in between the particles should be expected, due to the relatively fast flow of air through the bed and the hygroscopic nature of couscous. Nevertheless, the verification of absence of free water is crucial for the interpretation of the results, as detailed later.

It should be mentioned that Eq. (2) is a simplified version of the approach to analyse TD-NMR results presented by Trezza, Haiduc, Goudappel, and Van Duynhoven (2006). Using more than three components to fit the relaxation decays does not reduce the residual signal. We therefore conclude that fitting with a Gaussian, an exponential and one constant is adequate to describe the data.

Once the S, L and F contribution is determined, the total proton signal is computed as their sum. This allows for the study of the moisture content evolution, which can be quantitatively evaluated by scaling the $S + L + F$ value increase with respect to the sample mass gain.

2.3. X-ray tomography

2.3.1. Experimental procedure

The couscous particles are sieved to obtain a monodispersed size distribution, to simplify the image analysis procedure detailed later. Only particles collected in between 625 μm and 800 μm openings are used. It should be mentioned that this sieving procedure is only performed prior the X-ray tomography test, and not the TD-NMR campaigns. The particles are then kept at 13% RH air in a sealed vessel and are "dried" for 3 days, until they reach equilibrium with the surrounding environment. A lower level of RH could not be set due to technical limitations.

The particles are then transferred to a cylindrical PTFE cell (inner diameter d = 16 mm), above a high porosity ceramic stone. This functions as a diffusive filter, to provide homogeneous exposure to the flow coming from the bottom, while preventing particles from falling into the bottom channel connecting the cell to the RH control chamber. The chamber contains a potassium sulphate salt solution (120 g of $K{-}2SO_4$ and 1000 g of H_2O, 0.69 M molarity). This solution generates humidity in the air and maintains it at a rather constant 97% RH at a the room temperature of 24 ± 1 °C (Greenspan et al., 1977; Winston & Bates, 1960). Air is circulated from the RH control chamber to the bottom of the cell, through the sample and back to the chamber by means of a peristaltic pump. The flow rate is set to 0.2 L/min, a relatively fast flow, similar to the one above (Section 2.2.1). The experiment is performed once due to restricted access to the X-ray tomograph. A schematic overview of the experimental setup and procedure is shown in Fig. 2.

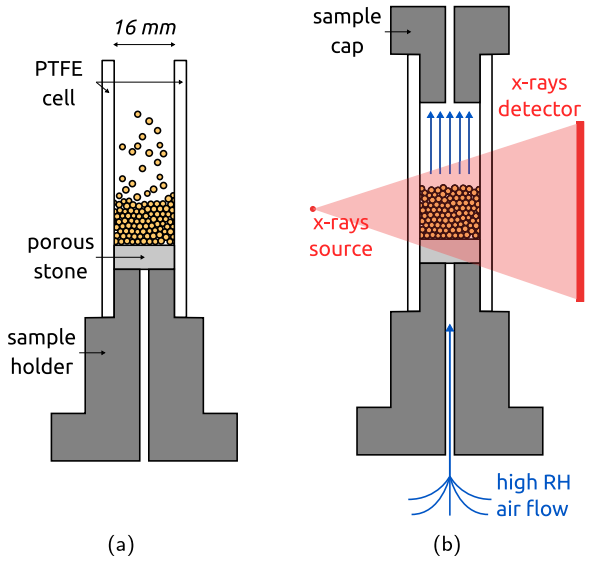

Fig. 2. Schematic view of the X-ray tomography experimental setup (a). The particles were poured in a rigid PTFE cell, above a porous stone, which functioned as a diffusive filter for the high RH air flow incoming from the bottom. The cell was sealed from top. The particles were exposed to high humidities, and X-ray tomographies were simultaneously acquired (b).

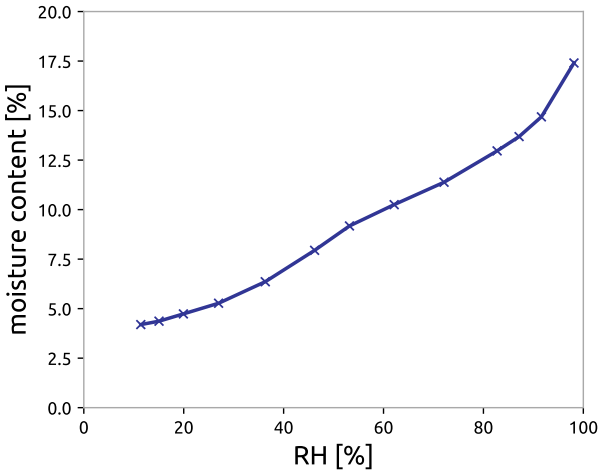

Fig. 3. Sorption isotherm of couscous particles at 20.7 °C. The particles are exposed step-wise to increasing RH and their weight is recorded to evaluate the moisture content.

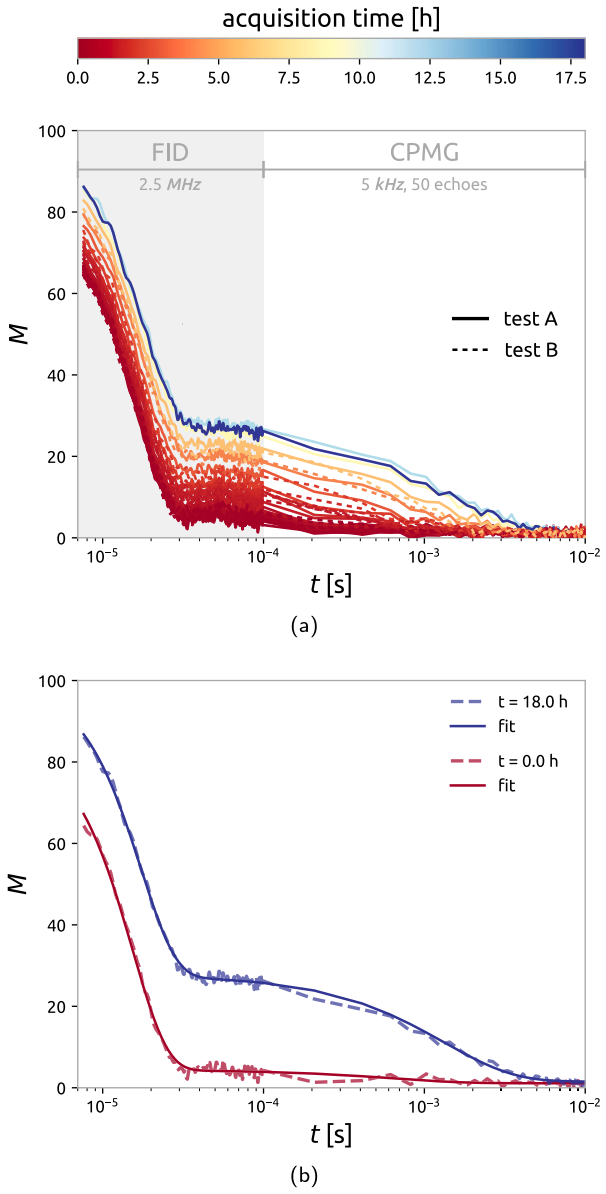

Fig. 4. (a) Magnetisation decay $M(t)$ obtained from the FID-CPMG sequence at different time-steps (from red to blue) throughout test A (plain lines) and test B (dashed lines). (b) Result of this interpolation with Eq. (2) of the first and last magnetisation decay $M(t)$ acquisitions of test A. (For interpretation of the references to colour in this figure legend, the reader is referred to the web version of this article.)

2.3.2. Imaging procedure

Tomographies are continuously acquired to capture the evolution of the sample's microstructure along time, employing the X-ray tomograph of the Laboratoire 3SR (Grenoble, France). The X-ray source is operated at 120 kV and 250 µA, and the pixel size is set to 17×2 µm, *i.e.*, 17 µm pixel size in binning 2. Each virtual, binned pixel collects the light of four neighbouring pixels, allowing for a faster image acquisition at the cost of a reduced spatial resolution. We select the binning 2 to increase the temporal resolution of the scans, an imperative choice considering the relatively high humid air flow rate and the ensuing speed of the process. The image 34 µm pixel size corresponds to an average of 20 pixels per particle diameter, which is deemed sufficient to segment and identify the grains, and characterise their volumetric deformation as detailed later in Section 3.3. Each tomography comprises 544 projections, each the result of the average of 10 acquisitions acquired at 10 Hz, lasting therefore approximately 10 min. A first, reference, tomography is acquired before the flow of high RH air is started. In total, 140 tomographies are acquired, which are then reconstructed with the Feldkamp filtered back projection algorithm (Feldkamp, Davis, & Kress, 1984) as implemented in the X-Act software by RX-solutions (Annecy, France).

3. Results and discussion

3.1. Sorption isotherm

Couscous is a hygroscopic material, thus it can absorb and release water from and into air. A common approach to characterise the water uptake of food is recording sorption isotherms (Erbaş, Ertugay, & Certel, 2005; Hebrard et al., 2003), which relates the material's relative increase of mass to the RH of the surrounding environment, all at constant temperature.

Fig. 3 shows the sorption isotherm of fine couscous particles, obtained by following the experimental procedure described in Section 2.1. This sorption isotherm resembles that of other durum wheat products, such as farina or semolina (Erbaş et al., 2005; Hebrard et al., 2003). The moisture content *m.c.* increases progressively for RH. Eventually, the absorption becomes significant for high RH, above 90%. The moisture content is at the beginning of the experiment equal to 4%, at 11% RH. It then increases up to 17.5% when the RH is 98%.

3.2. Water uptake and molecular mobility increase

TD-NMR is employed in this study to investigate the changes in ^{1}H proton signal intensity, *i.e.*, change in proton density and mobility (T_2) of the components. This allows for understanding how water vapour is sorbed by the couscous particles and whether molecular mobilisation occurs inside the solid matrix.

Fig. 4(a) shows evolution of the magnetisation decay $M(t)$ of both tests. At the onset of the experiment, the ^{1}H signal decays rapidly in the FID portion, while the signal almost completely disappears after 0.1 ms, indicating a strong glassy constitution. Later during the sorption process, part of the signal decays significantly slower. The slower decay is associated with a higher mobility of the protons within the sample, due to adsorption of water within the biopolymer matrix of the couscous particles.

The magnetisation decay is then interpolated with Eq. (2). Fig. 4(b) reports the results of this operation for the first and last $M(t)$ decay acquisitions of test A. Consequently, the contribution of solid-like S, liquid-like L and oil-like F components is determined. Their and the *total* signal ($S + L + F$) evolution with time are shown in Fig. 5(a). As expected, the total signal increases with time (solid lines), as progressively more water is absorbed by the particles. A slight decrease in the solid signal S (dashed lines) is observed. During the sorption process, water molecules may interact with protons in the solid matrix resulting in an increase of their relaxation time. As a result the $T_{2,S}$ of those protons in the solid fraction is shifting into the solid–liquid-like domain. The reduction of solid fraction signal S is complemented by the increase of the liquid-like one L (dash-dotted line). The oil signal F remains constant and minimal (dotted line), as expected.

The change of the average $T_{2,S}$ and $T_{2,L}$ with time is shown in Fig. 5(b). Both seem to increase monotonically. This suggests that the average molecular mobility increases with moisture content.

After approximately 12 to 13 h a steady state is reached, when the partial vapour pressure difference between the couscous particles and the humid air diminishes. This results in negligible net-change in water content and hence a plateau in the data. At this point the moisture content of the couscous particles is estimated from the relative weight gain over the experimental runs: 13.8% for test A and 13.2% for test B, assuming the particles to be close to dry (0% *m.c.*) after 3 days of drying at 0% RH.

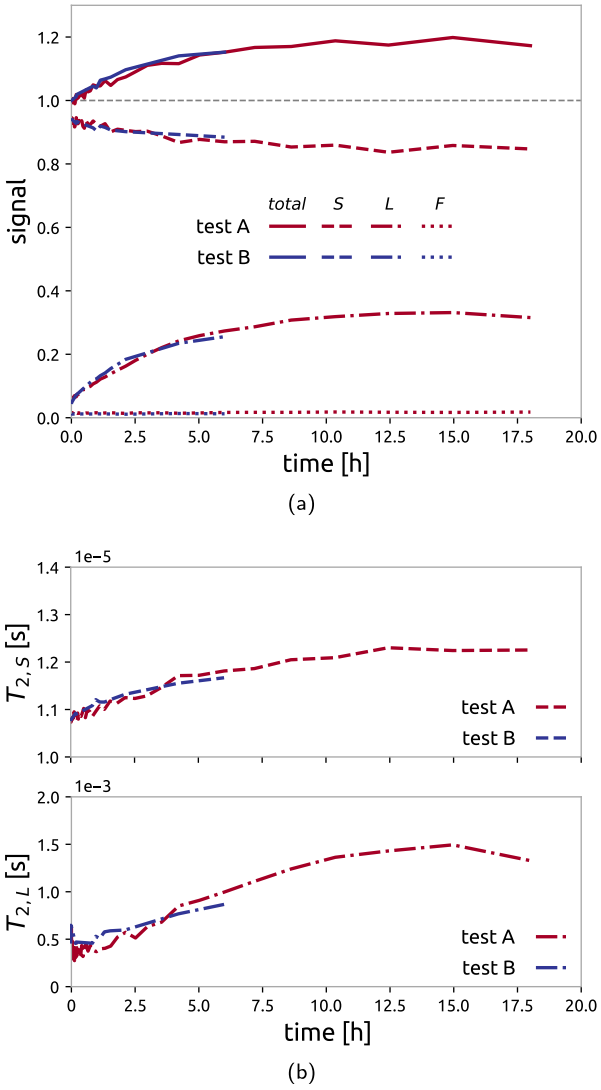

Fig. 5. Evolution with time of the solid fraction S, the liquid/semi-solid fraction L and the oil and mobile water fraction F (a). Increase with time of the T_2 relaxation times of the solid and liquid fractions S and L (b).

Vapour sorption mechanism –. During the TD-NMR experiments, the increase in moisture content, about 13.5%, is lower than expected, when compared to the gravimetric results (see Fig. 3). This can be explained by the difference in experimental conditions. The continuous flow of air through the packed bed limits the formation of liquid capillaries between the couscous particles, in contrast to the stationary gravimetric results (Liu, Wan, & Liu, 2021). This is confirmed by the absence of magnetisation decay signal associated with longer relaxation times (see Figs. 4(a) and 5(a)). It can be concluded that no free water is entrapped in the form of capillary bridges or water droplets. The F proton fraction does not increase over time, and all water vapour that is absorbed by the couscous is hence represented by L, with a short $T_{2,L}$ relaxation time of 1–1.5 ms.

Based on the results presented in the Appendix (see Fig. A.2(a)), it can be deduced that the experimental conditions do not limit the sorption rate by the influx of humid air at a flow-rate of 0.2 L/min. This is confirmed by the initial sorption rate in grams absorbed water per hour from the TD-NMR-data (see Fig. 10(a)), which is then compared to the mass flux of water vapour into the packed bed.

At the onset of test A the sorption rate is 9.8 mg/h, whereas, 0.2 g/h of water are supplied into the bed, a calculation based on a relative humidity of 97% at 0.2 L/min, and saturation water vapour concentration of 17 g/m^3. The ratio between the flux of water vapour into the bed and the initial sorption rate of the couscous particles is approximately 20. This suggests that the vapour sorption rate is diffusion limited, as the bed is over-supplied with water vapour. Therefore, the humidity of the air can safely be assumed constant over the packed bed.

Altogether, based on these results, it can be supposed that the couscous particles experience homogeneous air conditions. The water vapour is thereby expected to be absorbed uniformly though the bed. X-ray tomography is used to verify whether a uniform volumetric response is also observed thought the sample, as detailed below, since the particle deformation is expected to have a one-to-one relation with absorption.

3.3. Particles identification

The reconstructed 3D images represent the X-ray attenuation (and density) maps of the sample at different time-steps. As shown in Fig. 6(a), darker colours indicate a lower density material, such as air, while brighter colours are for the denser parts, *e.g.*, the ceramic porous stone. The vertical slices anticipate what is later discussed in Section 3.4: an increase in sample and particle volume.

The image analysis procedure for this data follows the one in our previous study (Vego et al., 2022), adopting functions and algorithms implemented in `spam`, an open source python based software for image analysis (Stamati et al., 2020).

First, the effects of spurious fluctuations in X-ray attenuation during the experiment are corrected. As shown in Fig. 6(b) for the representative tomography (at $t = 0$ h), from the gray-value distribution it is straightforward to identify the peaks corresponding to each component (air, couscous particle and cell (PTFE)) and the histogram is normalised between zero and one. We then impose the peak gray-values of air and cell to be constant throughout the entire experiment, as their attenuation is not supposed to change. All the other voxel gray-values are scaled accordingly. The couscous particles peak cannot be chosen for this operation, since it has been found that its gray-value is affected by increase of moisture content (Vego et al., 2022).

All the 140 tomographies are then "binarised", *i.e.*, the phases in the system are identified, classifying each image voxel in one phase category. The TD-NMR analysis procedure recognises the different components of the couscous solid fraction (S, L and F, see Section 2.2.3 and Eq. (2)). From X-ray tomography images, this distinction is not possible. Nonetheless, the spatial distribution of the solid and void phase in the sample can be identified[1]. This classification is based on whether the attenuation value is below or above a certain threshold, which is calculated via Otsu's method on the reference image (Otsu, 1979) (Fig. 6(b)). The result of this binarisation process is shown in Fig. 7(a) as a 3D rendering of the couscous sample.

Once the particles are identified it is possible to separate and assign them a unique label, *i.e.*, the value of each voxel belonging to a particle is set equal to an integer number. To perform the former, a distance map is computed, and its relative maxima are used as "flooding" points for the watershed algorithm (Beucher, 1982), as implemented in `spam`. We fixed the over- and under-labelling issues common in this kind of approach with the same software. In this case, we identified 8543 different particles. A 3D rendering of this labelled image is reported in Fig. 7(b).

[1] The internal pores of the particle are included into the solid phase fraction, to simplify the analysis.

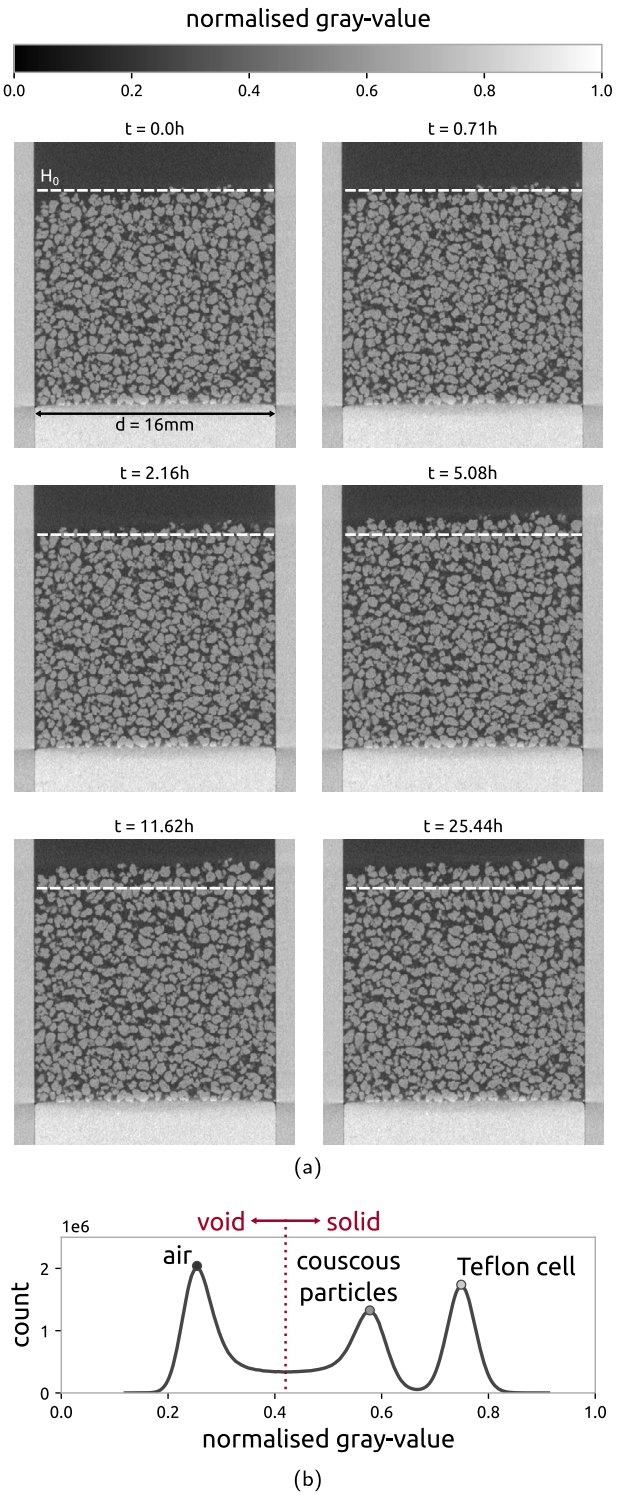

Fig. 6. Evolution of the sample along the test: vertical slices taken in the centre of the sample (d = 16 mm) of the reconstructed X-ray tomography images (a). The particles absorb water and swell and the sample height increases more than 1 mm. The histogram of the gray-values highlighting the attenuation of the main phases, normalised between zero and one (b).

3.4. Sample- and particle-scale volumetric response

The labelled image is essential to perform discrete digital volume correlation (dDVC). This technique has been used for the first time by Hall et al. (2010) (Hall et al., 2010) and is now implemented in

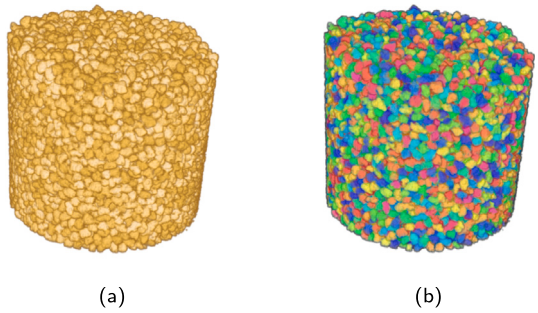

Fig. 7. 3D rendering of the image analysis operations of the reference images ($t = 0$ h) of the binary image (a) and labelled image (b) of couscous particles. The labelling procedure revealed the presence of 8543 particles, and to each of them a unique integer value is assigned.

`spam` (Dijkstra, Andò, & Dano, 2019). It employs the labelled image to extract reference sub-volumes for each particle and perform a digital volume correlation on them, between the reference and "deformed" configurations. This provides a deformation function for each particle, *i.e.,* their 3D displacement and internal deformation, with sub-voxel accuracy. The particle position and its deformation is measured at each time-step (Stamati et al., 2020; Vego et al., 2022). Convergence is not reached for only a negligible number of particles (always lower than 0.28% of the total).

The volumetric strain of the sample $\varepsilon_{V,s}$ is computed as the ratio between the sample height variation at time t and the reference one ($t = 0$ h). Only the vertical strain is considered since the cell's geometry prevents any radial swelling of the sample. The sample dilates up to 11.3% throughout the test.

The volume of each particle is calculated as the sum of all the voxels characterised by the same label. Then, the diameter on a volume-equivalent sphere is measured. The resulting average particle diameter in the sample at the beginning of the experiment is 0.71 ± 0.07 mm, in line with the sieving procedure adopted (Section 2.3.1).

The particle volumetric strain $\varepsilon_{V,p}$ can then be measured as the ratio between the particle volume variation and their initial volume (Vego et al., 2022). Overall, the particles swell by 9% by the end of the test. The evolution of the particle size distribution with sorption is presented and discussed in the (Appendix B)

Fig. 8(a) reports the evolution of the volumetric strain of the sample $\varepsilon_{V,s}$ as well as of the average one of the particles $\bar{\varepsilon}_{V,p}$ and its standard error. A similar amount of particle and sample volumetric strain could be expected. Nonetheless, since radial strain is prevented, the constrained particles rearrange, inducing a larger sample dilation than the average particle swelling. It is interesting to observe that after about 12–13 h the swelling plateaus, as particles likely reach a steady state with the external environment, similarly to the total signal in the TD-NMR experiment, see Section 3.2.

The relation between $\bar{\varepsilon}_{V,p}$ and $\varepsilon_{V,s}$ is found to be (quasi-)linear, as shown in Fig. 8(b). Without constraints in the vertical direction, the sample is free to increase in volume together with individual particles swelling, albeit at a different rate.

Pressure induced heterogeneity –. Based on the results discussed in Section 3.2, an homogeneous swelling response of the media and no water condensation should be expected, specifically due to the relatively fast flow of high RH air. The X-ray tomography is conducted under similar conditions as the TD-NMR, although on a larger sample (see Sections 2.2.1 and 2.3.1). The initial mass of the sample is in fact 2.32 g. After 25 h exposure to 97% RH air, the particles absorb 0.21 g of water. Then, the sample is dried in a convection oven for 24 h at 105 °C, indicating a 4% initial moisture content, which is in agreement with the sorption isotherm and the drying prior testing at 13% RH. Based

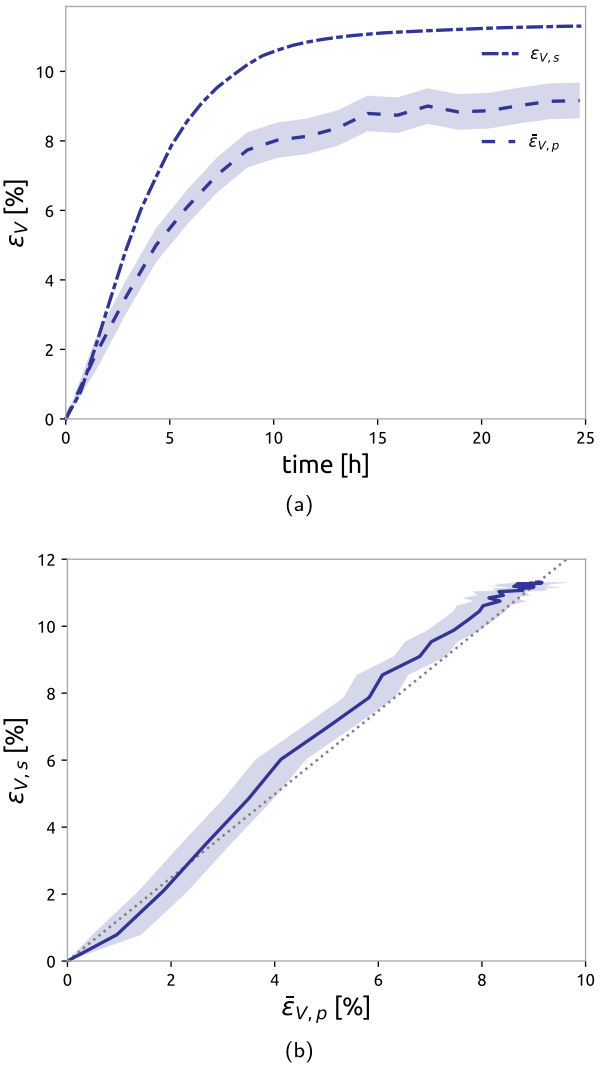

Fig. 8. Evolution of the sample volumetric strain $\varepsilon_{V,s}$ and the average particle volumetric strain $\bar{\varepsilon}_{V,p}$ in time with its standard error (a). The particles absorb water from the external environment and swell. This causes a dilation along the vertical direction of the overall sample as the particles rearrange. Relation between $\varepsilon_{V,s}$ and $\varepsilon_{V,s}$ (b). The dilation of the sample is nearly linearly proportional to particle swelling.

on this measure, the final moisture content is deduced to be 13.4%, a value analogous to the one recorded in the two TD-NMR campaigns.

The particle vertical displacement map throughout the entire test is then investigated. As highlighted in Fig. 9(a), a significant influence of the boundary conditions is found. Ideally, in unconstrained conditions, the swelling induced displacement should be horizontally uniform. However, lower displacement is measured for particles close to the rigid cylinder wall, limited by friction and arching once the particles start to swell and "push" each other.

Next, the spatial distribution of the particle volumetric strain $\varepsilon_{V,P}$ across the sample is investigated. As shown in Fig. 9(b), the swelling is found to have a gradient along the vertical axis. The particles at the bottom of the sample dilate earlier than the upper ones. This swelling gradient is particularly visible in the intermediate phase of the experiment (in Fig. 9(b), $t = 2.16$ h and $t = 5.08$ h), while by its end the particles seem to reach a stable maximum swelling capacity for the applied RH level (Fig. 8(a)).

As mentioned, a homogeneous particle swelling through the sample is expected occur. Taking into account the higher initial mass of the sample, within the first hour, 300% the water needed to saturate the system is supplied by the humid air flow. Nevertheless, a gradient is clearly measured, suggesting strongly that the water absorption is not

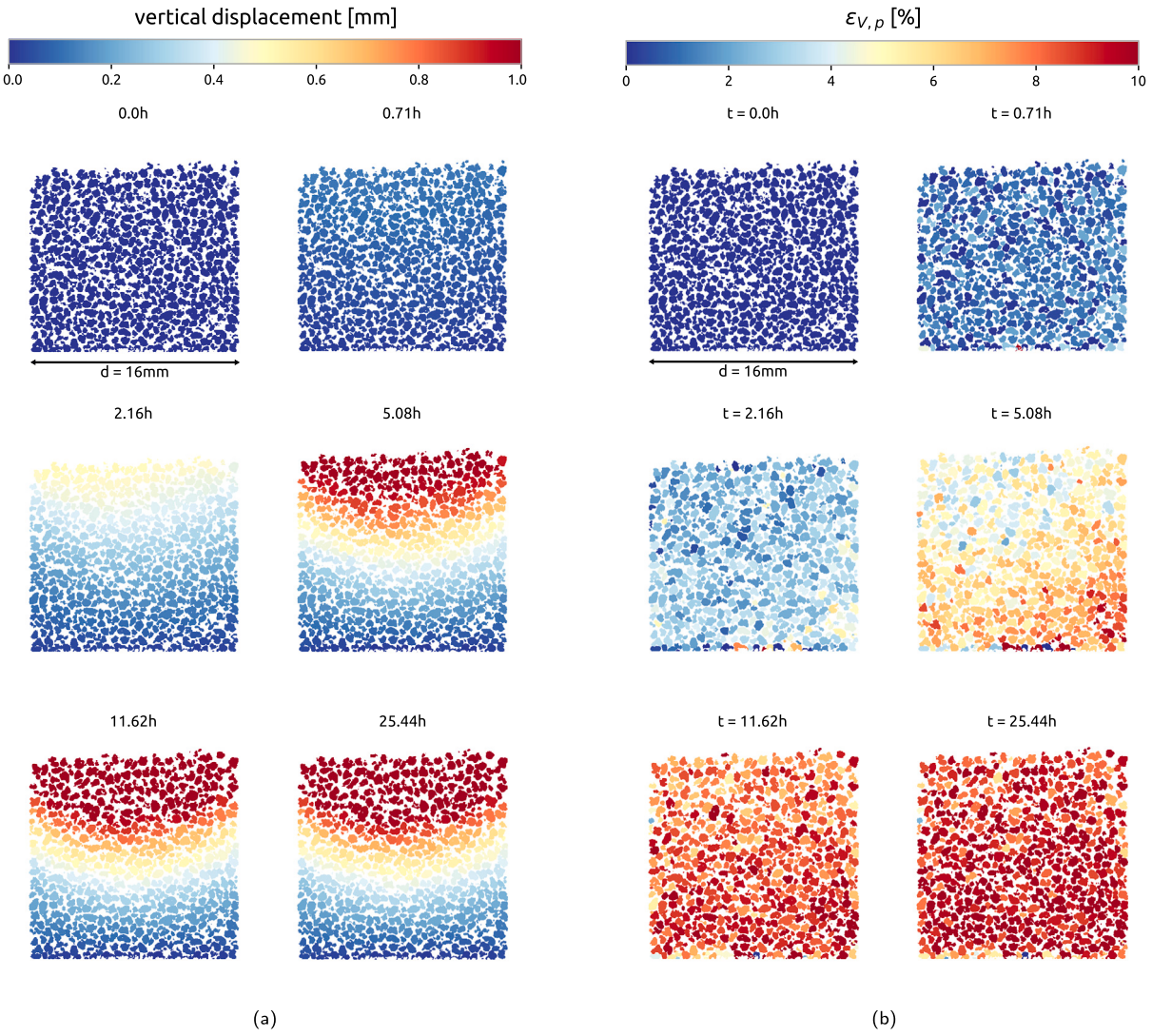

Fig. 9. Vertical slices of the particle vertical displacement (a) and volumetric strain $\varepsilon_{V,p}$ (b) 3D maps. From the vertical displacement map it can be observed how the radial constraints limited the displacement of particles close to the outer boundary. A pressure induced swelling gradient is detected in the intermediate time-steps despite the over-supply of water vapour by the fast flow of humid air. By the end of the test, all particles swell by roughly the same amount.

only dependent on water vapour concentration, *i.e.*, mass of water per volume. Naively, one would perhaps expect that with homogeneous absorption conditions, higher swelling should be measured in the upper regions, where the mechanical constrains are less severe, as suggested by the vertical displacement maps (Fig. 9(a)). Higher inter-particle forces would in fact prevent outward swelling and induce closing of internal pores. On second thought, we can explain the higher particle dilation (hence, absorption) due to the effects of pressure. As the air flows through the couscous assembly, a pressure gradient is inevitably generated (Carman, 1997). In the past, it has been found that air pressure can significantly affect the maximum amount of water that a material can entrap (He, Ng, Yap, & Saha, 2009; Schmidt, 2004), when the difference is in the order of 10 kPa. In our case, we estimate the air pressure drop from bottom to top three orders of magnitude lower (Carman, 1997), quite a small pressure difference, but strong enough to affect the absorption dynamics. Initially, the stronger pressure at the bottom induces a higher vapour pressure, thus a quicker water absorption. This swelling heterogeneity fades in the late stages of the test, as the particle absorption and dilation capacity is reached.

The results also suggest the additional presence of a horizontal gradient (see Fig. 9(b)). This is likely produced by small gaps between porous stone and rigid cell, which can create preferential air flow paths. Thus, the pressure distribution is not homogeneous horizontally, and consequently neither are absorption and swelling. Nevertheless, the rather homogeneous swelling spatial distribution in the late stages of the test suggest that the magnitude of the horizontal air pressure gradient is in the order of magnitude of the vertical one previously estimated.

In a previous work, a swelling gradient was found as well (Vego et al., 2022). In that case, couscous particles were also exposed to 97% RH air flow, but the flow was 10 times slower. In retrospect, it cannot be excluded that the heterogeneity in the previous experiment was prompted by the insufficient air water concentration, besides a pressure difference. Moreover, condensation of water cannot be ruled out due the lower flow rate.

3.5. Free swelling and moisture content relation

Next, the relation between the volumetric response of couscous and water absorption behaviour is investigated.

While it is not possible to perform the TD-NMR and the tomography tests at the same time, the two are performed in similar conditions and the final mass variations are equivalent, as detailed above, hence correlations can be established between moisture content and volumetric strain.

A small difference in the initial relative humidity of the materials is nonetheless present in the two tests. As mentioned in Section 2.2.1, before the TD-NMR tests, the particles are dried for 3 days at 0% RH, which should induced a moisture content *m.c.* close to 0%. The increment measured through TD-NMR coincides then to a 13.8% final moisture content of test A. In the free swelling experiment with X-ray tomography, the initial moisture content is determined equal to 4%. For this reason, we correlate here the particle swelling to the TD-NMR data only after 4% moisture content is exceeded in the latter. The so adjusted evolution in time of the moisture content *m.c.* from TD-NMR signal increment and the average particle swelling $\bar{\varepsilon}_{V,p}$ from X-ray tomography are shown in Fig. 10(a), by red and blue points respectively.

Both variables appear to follow an exponential growth equation:

$$x(t) = X\left(1 - e^{-\frac{t}{\tau_0}}\right) \tag{3}$$

where X and τ_0 are two constants characteristic of the material. This model has been found to be a good fit for the sorption behaviour of super-absorbent polymers by Omidian, Hashemi, Sammes, and Meldrum (1998) and a recent study showed that it can accurately describe the swelling dynamics of couscous under extreme conditions such as submerged particles (De Richter et al., 2022).

Eq. (3) can be used to describe the water uptake (and thus the moisture content *m.c.*) as well as the average particle volumetric strain. While τ_0 remains an unknown of the problem, X is simply the asymptotic limit of the plateau. Consequently, the two following Equations describe respectively the water uptake and the average particle swelling:

$$m.c.(t) = m.c._{MAX}\left(1 - e^{-\frac{t}{\tau_{mc,0}}}\right) \tag{4}$$

$$\bar{\varepsilon}_{V,p}(t) = \bar{\varepsilon}_{V,p,MAX}\left(1 - e^{-\frac{t}{\tau_{\varepsilon,0}}}\right) \tag{5}$$

These Equations accurately reproduce the experimental results, as shown in Fig. 10(a) (plain blue and red lines).

When particle swelling and moisture content increase are compared it is found that the relation between these two variables can be described by a (quasi-)linear relation, as shown in Fig. 10(b).

The influence of the swelling gradient on the linear coefficient is investigated. The results show a slight increase of the inclination by taking into account only the lower regions of the sample, which is however within measurement sensitivity interval. As an example, Fig. 10(b) reports the evolution for the case in which only the swelling of particles below 1/4 the initial height of the sample are taken into consideration, and the moisture content is still treated as a global variable.

It should be noted that this linearity could be lost in case of water condensation or presence of droplets, as suggested by De Richter et al. (2022). The presence of liquid water causes the formation of a gelatinous layer that can decrease the diffusion and, thus, the absorption rate of the internal regions of the particles. Nevertheless, the presence of unbound water can be excluded in this study case. The TD-NMR results do not show a signal from highly mobile ^{1}H protons (see Figs. 4(a) and 5(a)). It can be inferred the same for the complementary campaign, owing to equivalent moisture content by the end of all tests.

4. Conclusions and perspectives

Using TD-NMR relaxometry we observe the change in molecular mobility from the increase of the characteristic T_2 relaxation time, as well as the decrease in solid-like signal S and the increase of the bound water signal L. No increase of the signal F of unbound water and oil is observed as the relatively fast flow of air prevents the formation of liquid bridges by capillary condensation.

X-ray tomography allows us to quantify the sample dilation and the volumetric strain of the vast majority of the 8543 particles. The

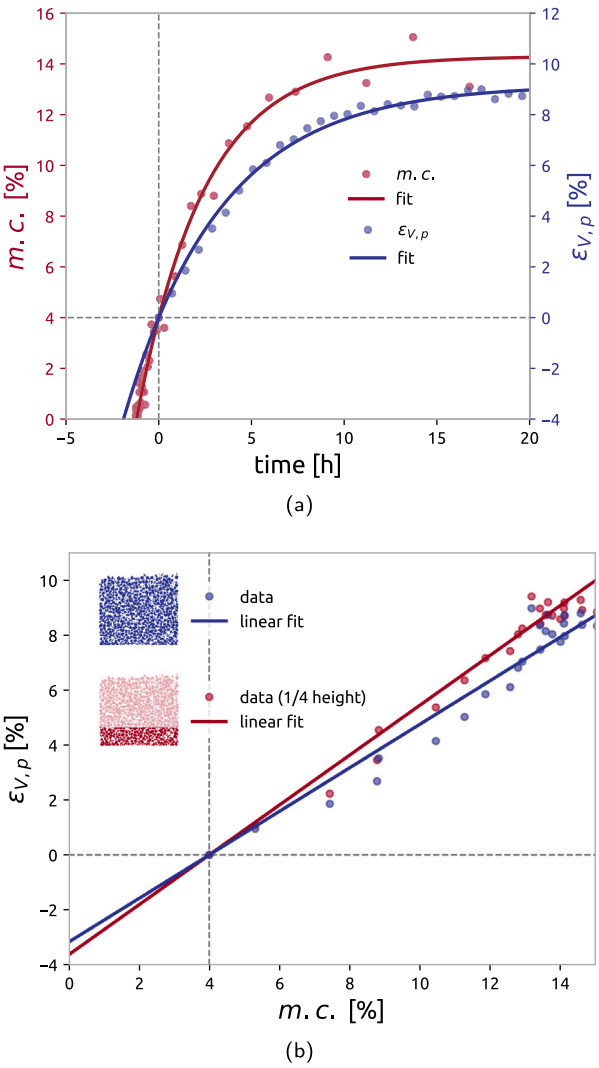

Fig. 10. Evolution with time of the moisture content (in red) and of the particle swelling (in blue) both plateauing (a). Linear relation between particle volumetric strain $\varepsilon_{V,p}$ and moisture content *m.c.* extracted from experimental data (b). The $\varepsilon_{V,p}$ and *m.c.* experimental curves with time are interpreted through Eq. (3). A slight effect of the swelling gradient is observed on the linear coefficient describing the $\varepsilon_{V,p}$ and *m.c.* relation. (For interpretation of the references to colour in this figure legend, the reader is referred to the web version of this article.)

volumetric response shows a similar pattern to the sorption determined by TD-NMR, approaching steady state after about 12–13 h at both the particle- and sample-scale.

A modest swelling gradient is observed despite the homogeneous water concentration in the air provided by the relatively fast flow of humid air. This can be explained by gradients inducing a small pressure difference, which in turn influences locally the sorption rate (He et al., 2009; Schmidt, 2004).

A coherent mass gain (*i.e.*, overall change of moisture content) between the TD-NMR and X-ray tomography tests allows us to link the water uptake and the particle swelling in the two tests. The sorption and volumetric response follows the exponential growth model, similarly to other hygroscopic materials (De Richter et al., 2022; Omidian et al., 1998). The relation between particle volumetric strain and moisture content increase is found to be (quasi-)linear.

Future research should focus on understanding the physical meaning of the free variable τ_0 in Eq. (3), and on the effect of different boundary conditions, *e.g.*, isochoric and oedometric. In future works we will explore the spatial distribution of water in the sample, and its

effects on the material micro-structure by means of simultaneous neutron and X-ray tomography. A multi-scale mechanical characterisation of the material could complement the morphological information, and provide essential information to understand the underlying phenomena of particles agglomeration and caking. This would also benefit the eventual development and calibration of numerical models aimed at investigating the role played by variables difficult to control or directly measure experimentally.

CRediT authorship contribution statement

Ilija Vego: Conceptualization, Methodology, Software, Validation, Formal analysis, Investigation, Writing – original draft, Visualization. **Richard T. Benders:** Conceptualization, Methodology, Validation, Investigation, Writing – original draft. **Alessandro Tengattini:** Methodology, Validation, Data curation, Writing – review & editing, Supervision. **Frank J. Vergeldt:** Software, Validation, Formal analysis, Investigation, Resources, Writing – review & editing. **Joshua A. Dijksman:** Conceptualization, Methodology, Resources, Writing – review & editing, Supervision, Project administration, Funding acquisition. **John P.M. van Duynhoven:** Validation, Formal analysis, Resources, Writing – review & editing, Supervision.

Declaration of competing interest

The authors declare that they have no known competing financial interests or personal relationships that could have appeared to influence the work reported in this paper.

Acknowledgements

We are thankful to Remco Fokkink, Gert-Jan Goudappel, and Hans de Rooij for the technical support and we thank Julia Veser for the fruitful discussions during the TD-NMR experimental campaigns. We acknowledge the MAGNEFY NMR facility, which is supported by uNMR-NL, the National Roadmap Large-Scale Facility of the Netherlands (NWO grant 184.032.207). We are grateful to Gioacchino Viggiani and Edward Andò for the advice on the image analysis approach and interpretation of results. We thank Pascal Charrier and Nicolas Lenoir for the technical support with X-ray tomographies acquisition. The Laboratoire 3SR is part of the LabEx Tec 21 (Investissements dAvenir – grant agreement n-11-LABX-0030). This project has received funding from the European Unions Horizon 2020 research and innovation program under the Marie Skłodowska-Curie grant agreement no. 812638 (CALIPER).

Appendix A. Benchtop NMR experiments: Effects of flow rate and RH on sorption

Prior to the TD-NMR relaxometry campaign presented in Section 2.2, a series of tests is carried out to settle the optimal experimental conditions. The tests are performed using a spectrometer (Pure Devices MagSpec 23 MHz, 0.55 T), different from the Bruker MiniSpec detailed previously. The same measurement cell as above is used. In order to optimise the data acquisition and achieve high temporal resolution of the hydration process (≈500 hundred in one day), we compromise the time interval extent describing the signal decay.

Fig. A.1 presents a comparison between the FID-CPMG signal decays obtained by the two spectrometers. With the chosen PD acquisition settings, the sequence decay of the solid fraction is not observed in its entirety. Nonetheless, a good agreement is found between spectrometers for longer T_2 relaxation times. While the chosen setting do not allow for studying directly the solid fraction, the vapour-sorption is analysed from the semi-solid tail and liquid-like fractions contribution on the decay curve (> 0.1 ms).

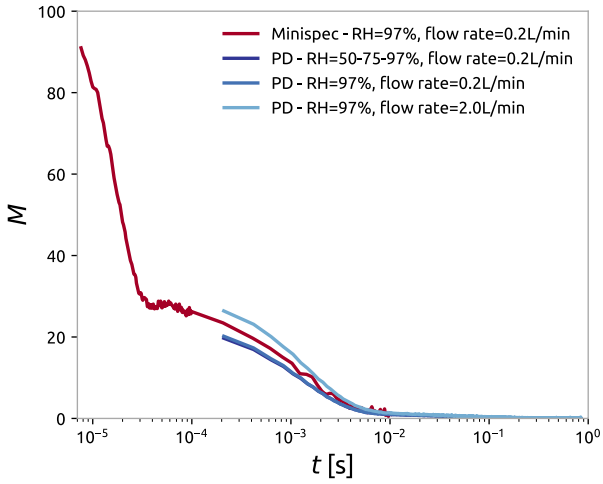

Fig. A.1. Comparison between FID-CPMG and CPMG magnetisation decays $M(t)$ obtained from the two experimental campaigns. Representative decay curves at the end of tests are compared. While only the chosen MiniSpec acquisition optimisation allow for capturing the signal of the less mobile protons in the system (solid fraction), both devices agree on the more mobile fraction (semi-solid/liquid phase).

Fig. A.2(a) shows the effect of 2 different air velocities on the relative sorption rate, highlighting a negligible effect, despite 1 order of magnitude of difference in flow rate. This indicates that the process was likely limited by the diffusion of water inside the couscous particles themselves rather than the flow rate across the sample.

Furthermore, the sorption signal is analysed at different RH-levels over time (see Fig. A.2(b)). Starting with a RH of 50%, a steady state is reached after approximately 12 h, next the RH was increased to 75% after which more water vapour was absorbed by the couscous particles. Finally, after 20 h, the RH is tuned to 97%, and another steady state plateau is observed after 11–12 h. The relative increments in amount of water at the different RH levels, concur with the gravimetric study results presented in Section 2.1.

A.1. Conclusions

From these experiments the effects of two different variables in the couscous particles hydration problem are explored. The analysis of the semi-solid tail and liquid-like fractions reveals that there exist a fast flow regime, where the effect of flow rate does not influence the absorption process. Furthermore, the role played by the RH level in the sorption process is investigated. The moisture content (total signal) increases for higher RH, as expected, and it is in agreement with gravimetric studies. Moreover, a plateau is reached after about 12 h, similarly to the other tests presented above.

Appendix B. Evolution of the size distribution with water sorption

Particle size distribution (PSD) is a common way of analysing physical properties of granular materials and their change upon mechanical loading or chemical reactions.

As mentioned Section 3.3, the analysis of X-ray tomography images allows for the tracking of thousands of particles with DVC and the generation of sequential labelled images. These provide information about the geometry of all particles in the sample and its evolution with time. It is therefore possible to produce PSD curves directly *via* image analysis, bypassing the more classical sieving method.

Using the dedicated function implemented in the `spam` software (Stamati et al., 2020) distributions are obtained from different sequential labelled images, after computing the equivalent diameter of all particles, as shown in Fig. B.1. First, it can noticed how the results

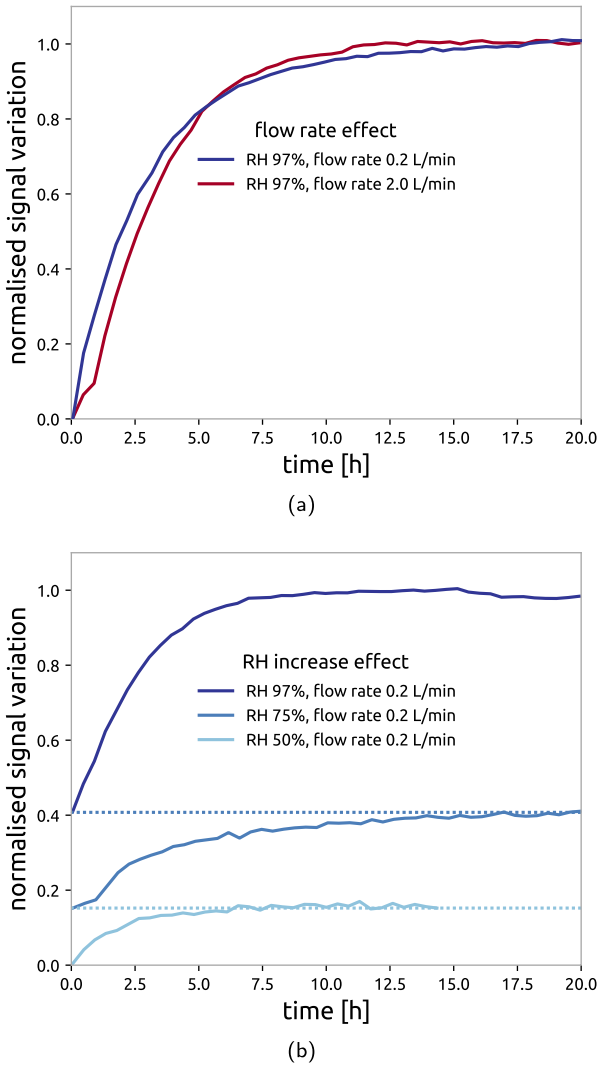

Fig. A.2. Effects of flow rate (a) and RH (b) from the PD CPMG signal (moisture content). The signal plateaus at 12–13 h. No significant effect is observed for two different flow rates, despite one order of magnitude variation. An experiment is performed on the same material for multiple days while the RH is increased progressively once the material reaches a steady state with the external environment. The signal, thus the moisture content, increases upon increasing the RH from 50 to 75 and, finally, to 97%.

are consistent with the sieving procedure prior the X-ray tomography test (see Section 2.3.1). At the beginning of the test, the vast majority of particles is within the 625 μm and 800 μm range and the distribution is relatively monodispersed. With time, thus with increasing moisture content, the PSD shifts to the right, as the particles swell. Moreover, it can be observed how the size increase is stronger in the initial steps, when the sorption rate is higher (see Fig. 10(a)).

B.1. Conclusions

The analysis of the PSD confirms a significant swelling of couscous particles with water sorption. The curves, taken at different time-steps, highlight the size increase of the particles and are consistent with the sieving procedure adopted in the sample preparation.

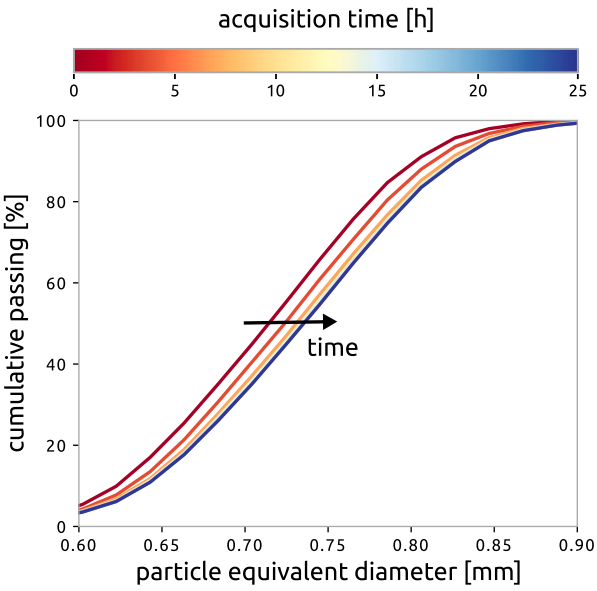

Fig. B.1. Cumulative passing particle size distribution at different times obtained from the analysis of the labelled X-ray tomography images.

References

Abecassis, J., Cuq, B., Boggini, G., & Namoune, H. (2012). Other traditional durum-derived products. In *Durum wheat chemistry and technology* (pp. 177–199). Springer, http://dx.doi.org/10.1016/B978-1-891127-65-6.50015-5.

Aguilera, J., del Valle, J., & Karel, M. (1995). Caking phenomena in amorphous food powders. *Trends in Food Science & Technology*, *6*(5), 149–155. http://dx.doi.org/10.1016/S0924-2244(00)89023-8.

Amin, M., Hossain, M., & Roy, K. (2004). Effects of moisture content on some physical properties of lentil seeds. *Journal of Food Engineering*, *65*(1), 83–87. http://dx.doi.org/10.1016/j.jfoodeng.2003.12.006.

Bellocq, B., Ruiz, T., & Cuq, B. (2018). Contribution of cooking and drying to the structure of couscous grains made from durum wheat semolina. *Cereal Chemistry*, *95*(5), 646–659. http://dx.doi.org/10.1002/cche.10078.

Beucher, S. (1982). Watersheds of functions and picture segmentation. In *ICASSP'82. IEEE international conference on acoustics, speech, and signal processing, vol. 7* (pp. 1928–1931). IEEE, http://dx.doi.org/10.1109/ICASSP.1982.1171424.

Brockbank, K., Armstrong, B., & Clayton, J. (2021). Measurement and quantification of caking in excipients and food products with emphasis on the non-homogeneous interaction with ambient moisture. *Particuology*, *56*, 75–83. http://dx.doi.org/10.1016/j.partic.2020.10.012.

Cao, W., Nishiyama, Y., & Koide, S. (2004). Physicochemical, mechanical and thermal properties of brown rice grain with various moisture contents. *International Journal of Food Science & Technology*, *39*(9), 899–906. http://dx.doi.org/10.1111/j.1365-2621.2004.00849.x.

Carman, P. C. (1997). Fluid flow through granular beds. *Chemical Engineering Research and Design*, *75*, S32–S48. http://dx.doi.org/10.1016/S0263-8762(97)80003-2.

Carpin, M., Bertelsen, H., Bech, J., Jeantet, R., Risbo, J., & Schuck, P. (2016). Caking of lactose: A critical review. *Trends in Food Science & Technology*, *53*, 1–12. http://dx.doi.org/10.1016/j.tifs.2016.04.002.

Carr, H. Y., & Purcell, E. M. (1954). Effects of diffusion on free precession in nuclear magnetic resonance experiments. *Physical Review*, *94*, 630–638. http://dx.doi.org/10.1103/PhysRev.94.630.

Chauhan, C., Dhir, A., Akram, M. U., & Salo, J. (2021). Food loss and waste in food supply chains. A systematic literature review and framework development approach. *Journal of Cleaner Production*, *295*, Article 126438. http://dx.doi.org/10.1016/j.jclepro.2021.126438.

Chung, M. S., Ruan, R., Chen, P., Chung, S. H., Ahn, T. H., & Lee, K. H. (2000). Study of caking in powdered foods using nuclear magnetic resonance spectroscopy. *Journal of Food Science*, *65*(1), 134–138. http://dx.doi.org/10.1111/j.1365-2621.2000.tb15968.x.

Crouter, A., & Briens, L. (2014). The effect of moisture on the flowability of pharmaceutical excipients. *Aaps PharmSciTech*, *15*(1), 65–74.

De Richter, S. K., Gaudel, N., Gaiani, C., Pascot, A., Ferrari, M., & Jenny, M. (2022). Swelling of couscous grains under saturated conditions. *Journal of Food Engineering*, *319*, Article 110910. http://dx.doi.org/10.1016/j.jfoodeng.2021.110910.

Dijkstra, J., Andò, E., & Dano, C. (2019). Grain kinematics during stress relaxation in sand: Not a problem for X-ray imaging. In *E3S web of conferences: vol. 92*, (p. 01001). EDP Sciences, http://dx.doi.org/10.1051/e3sconf/20199201001.

Erbaş, M., Ertugay, M. F., & Certel, M. (2005). Moisture adsorption behaviour of semolina and farina. *Journal of Food Engineering*, *69*(2), 191–198. http://dx.doi.org/10.1016/j.jfoodeng.2004.07.017.

Feldkamp, L. A., Davis, L. C., & Kress, J. W. (1984). Practical cone-beam algorithm. *Josa A*, *1*(6), 612–619. http://dx.doi.org/10.1364/JOSAA.1.000612.

Figueroa, J., Hernández, Z., Véles, M., Rayas-Duarte, P., Martínez-Flores, H., & Ponce-García, N. (2011). Evaluation of degree of elasticity and other mechanical properties of wheat kernels. *Cereal Chemistry*, *88*(1), 12–18. http://dx.doi.org/10.1094/CCHEM-04-10-0065.

Fitzpatrick, J. J., & Ahrné, L. (2005). Food powder handling and processing: Industry problems, knowledge barriers and research opportunities. *Chemical Engineering and Processing: Process Intensification*, *44*(2), 209–214. http://dx.doi.org/10.1016/j.cep.2004.03.014.

Glenn, G., Younce, F., & Pitts, M. (1991). Fundamental physical properties characterizing the hardness of wheat endosperm. *Journal of Cereal Science*, *13*(2), 179–194. http://dx.doi.org/10.1016/S0733-5210(09)80035-0.

Greenspan, L., et al. (1977). Humidity fixed points of binary saturated aqueous solutions. *Journal of Research of the National Bureau of Standards*, *81*(1), 89–96. http://dx.doi.org/10.6028/jres.081A.011.

Hahn, E. L. (1953). Free nuclear induction. *Physics Today*, *6*(11), 4–9. http://dx.doi.org/10.1063/1.3061075.

Haider, C. I., Hounslow, M. J., Salman, A. D., Althaus, T. O., Niederreiter, G., & Palzer, S. (2014). Influence of environmental conditions on caking mechanisms in individual amorphous food particle contacts. *AIChE Journal*, *60*(8), 2774–2787. http://dx.doi.org/10.1002/aic.14490.

Hall, S. A., Bornert, M., Desrues, J., Pannier, Y., Lenoir, N., Viggiani, G., et al. (2010). Discrete and continuum analysis of localised deformation in sand using X-ray μCT and volumetric digital image correlation. *Géotechnique*, *60*(5), 315–322. http://dx.doi.org/10.1680/geot.2010.60.5.315.

Hammami, R., Barbar, R., Laurent, M., & Cuq, B. (2022). Durum wheat couscous grains: An ethnic Mediterranean food at the interface of traditional domestic preparation and industrial manufacturing. *Foods*, *11*(7), 902. http://dx.doi.org/10.3390/foods11070902.

Hammami, R., & Sissons, M. (2020). Durum wheat products, couscous. In *Wheat quality for improving processing and human health* (pp. 347–367). Springer, http://dx.doi.org/10.1007/978-3-030-34163-3_15.

Hatzakis, E. (2019). Nuclear magnetic resonance (NMR) spectroscopy in food science: A comprehensive review. *Comprehensive Reviews in Food Science and Food Safety*, *18*(1), 189–220. http://dx.doi.org/10.1111/1541-4337.12408.

He, J., Ng, K., Yap, C., & Saha, B. (2009). Effect of pressure on the adsorption rate for gasoline vapor on pitch-based activated carbon. *Journal of Chemical & Engineering Data*, *54*(5), 1504–1509. http://dx.doi.org/10.1021/je800809k.

Hebrard, A., Oulahna, D., Galet, L., Cuq, B., Abecassis, J., & Fages, J. (2003). Hydration properties of durum wheat semolina: Influence of particle size and temperature. *Powder Technology*, *130*(1–3), 211–218. http://dx.doi.org/10.1016/S0032-5910(02)00268-1.

Juarez-Enriquez, E., Olivas, G., Zamudio-Flores, P., Ortega-Rivas, E., Perez-Vega, S., & Sepulveda, D. (2017). Effect of water content on the flowability of hygroscopic powders. *Journal of Food Engineering*, *205*, 12–17. http://dx.doi.org/10.1016/j.jfoodeng.2017.02.024.

Kamst, G., Bonazzi, C., Vasseur, J., & Bimbenet, J. (2002). Effect of deformation rate and moisture content on the mechanical properties of rice grains. *Transactions of the ASAE*, *45*(1), 145. http://dx.doi.org/10.13031/2013.7857.

Liu, L., Wan, K. T., & Liu, K. K. (2021). Influence of relative humidity on interparticle capillary adhesion. *Langmuir*, *37*(43), 12714–12722. http://dx.doi.org/10.1021/acs.langmuir.1c02167.

Lumay, G., Traina, K., Boschini, F., Delaval, V., Rescaglio, A., Cloots, R., et al. (2016). Effect of relative air humidity on the flowability of lactose powders. *Journal of Drug Delivery Science and Technology*, *35*, 207–212. http://dx.doi.org/10.1016/j.jddst.2016.04.007.

Meiboom, S., & Gill, D. (1958). Modified spin-echo method for measuring nuclear relaxation times. *Review of Scientific Instruments*, *29*(8), 688–691. http://dx.doi.org/10.1063/1.1716296.

Morita, T., & Singh, R. P. (1979). Physical and thermal properties of short-grain rough rice. *Transactions of the ASAE*, *22*(3), 630–0636. http://dx.doi.org/10.13031/2013.35074.

Omidian, H., Hashemi, S., Sammes, P., & Meldrum, I. (1998). A model for the swelling of superabsorbent polymers. *Polymer*, *39*(26), 6697–6704. http://dx.doi.org/10.1016/S0032-3861(98)00095-0.

Otsu, N. (1979). A threshold selection method from gray-level histograms. *IEEE Transactions on Systems, Man, and Cybernetics*, *9*(1), 62–66. http://dx.doi.org/10.1109/TSMC.1979.4310076.

Penvern, H., Zhou, M., Maillet, B., Courtier-Murias, D., Scheel, M., Perrin, J., et al. (2020). How bound water regulates wood drying. *Physical Review Applied*, *14*, Article 054051. http://dx.doi.org/10.1103/PhysRevApplied.14.054051.

Rathore, A. S., & Winkle, H. (2009). Quality by design for biopharmaceuticals. *Nature biotechnology*, *27*(1), 26–34. http://dx.doi.org/10.1038/nbt0109-26.

Rostom, L., Courtier-Murias, D., Rodts, S., & Care, S. (2020). Investigation of the effect of aging on wood hygroscopicity by 2D 1H NMR relaxometry. *Holzforschung*, *74*(4), 400–411. http://dx.doi.org/10.1515/hf-2019-0052.

Sadeghi, M., Araghi, H. A., & Hemmat, A. (2010). Physico-mechanical properties of rough rice (*Oryza sativa L.*) grain as affected by variety and moisture content. *Agricultural Engineering International: CIGR Journal*, *12*(3–4), 129–136.

Schmidt, S. J. (2004). Water and solids mobility in foods. *Advances in Food and Nutrition Research*, http://dx.doi.org/10.1016/S1043-4526(04)48001-2.

Sharma, A. D., & Kunze, O. R. (1982). Post-drying fissure developments in rough rice. *Transactions of the ASAE*, *25*(2), 465–0468. http://dx.doi.org/10.13031/2013.33556.

Shi, L., Feng, Y., & Sun, C. C. (2011). Initial moisture content in raw material can profoundly influence high shear wet granulation process. *International Journal of Pharmaceutics*, *416*(1), 43–48. http://dx.doi.org/10.1016/j.ijpharm.2011.05.080.

Stading, M., Rindlav-Westling, Å., & Gatenholm, P. (2001). Humidity-induced structural transitions in amylose and amylopectin films. *Carbohydrate Polymers*, *45*(3), 209–217. http://dx.doi.org/10.1016/S0144-8617(00)00242-3.

Stamati, O., Andò, E., Roubin, E., Cailletaud, R., Wiebicke, M., Pinzon, G., et al. (2020). Spam: Software for practical analysis of materials. *Journal of Open Source Software*, *5*(51), 2286. http://dx.doi.org/10.21105/joss.02286.

Tabatabaeefar, A. (2003). Moisture-dependent physical properties of wheat. *International Agrophysics*, *17*(4), 207–211.

Trezza, E., Haiduc, A., Goudappel, G., & Van Duynhoven, J. (2006). Rapid phase-compositional assessment of lipid-based food products by time domain NMR. *Magnetic Resonance in Chemistry*, *44*(11), 1023–1030. http://dx.doi.org/10.1002/mrc.1893.

van Duynhoven, J., Voda, A., Witek, M., & Van As, H. (2010). Time-domain NMR applied to food products. *vol. 69*, In *Annual reports on NMR spectroscopy* (pp. 145–197). Elsevier, http://dx.doi.org/10.1016/S0066-4103(10)69003-5.

Vego, I., Tengattini, A., Andò, E., Lenoir, N., & Viggiani, G. (2022). Effect of high relative humidity on a network of a water-sensitive particles (couscous) as revealed by in-situ X-Ray tomography. *Soft Matter*, http://dx.doi.org/10.1039/D2SM00322H.

Virtanen, P., Gommers, R., Oliphant, T. E., Haberland, M., Reddy, T., Cournapeau, D., et al. (2020). SciPy 1.0: Fundamental algorithms for scientific computing in Python. *Nature Methods*, *17*, 261–272. http://dx.doi.org/10.1038/s41592-019-0686-2.

Wahl, M., Bröckel, U., Brendel, L., Feise, H., Weigl, B., Röck, M., et al. (2008). Understanding powder caking: Predicting caking strength from individual particle contacts. *Powder Technology*, *188*(2), 147–152. http://dx.doi.org/10.1016/j.powtec.2008.04.062.

Winston, P. W., & Bates, D. H. (1960). Saturated solutions for the control of humidity in biological research. *Ecology*, *41*(1), 232–237. http://dx.doi.org/10.2307/1931961.

Zafar, U., Vivacqua, V., Calvert, G., Ghadiri, M., & Cleaver, J. S. (2017). A review of bulk powder caking. *Powder Technology*, *313*, 389–401. http://dx.doi.org/10.1016/j.powtec.2017.02.024.